Atmospheric Environment 117 (2015) 51–60

Contents lists available at ScienceDirect

Atmospheric Environment

journal homepage: www.elsevier.com/locate/atmosenv

# Sources and formation pathways of organic aerosol in a subtropical metropolis during summer

I-Chun Tsai [a, b], Jen-Ping Chen [a, *], Candice Shi-Chun Lung [b], Nan Li [a, c], Wei-Nai Chen [b], Tzung-May Fu [d], Chih-Chung Chang [b], Gong-Do Hwang [a, e]

[a] Department of Atmospheric Sciences, National Taiwan University, Taipei, Taiwan
[b] Research Center of Environmental Changes, Academia Sinica, Taipei, Taiwan
[c] Key Lab of Aerosol Chemistry & Physics, Institute of Earth Environment, Chinese Academy of Sciences, Xi'an, China
[d] Department of Atmospheric and Oceanic Sciences and Laboratory for Climate and Ocean-Atmosphere Studies, Peking University, Beijing, China
[e] Taiwan Typhoon and Flood Research Institute, National Applies Research Laboratories, Taipei, Taiwan

## HIGHLIGHTS

- Biogenic contributions to OA formation are strong in both urban and rural Taipei.
- SOA dominated OA production, and its fraction increases with height in the PBL.
- Major contribution of OA from aqueous-phase processes.
- PBL height & sunlight variations and local circulation controlled OA diurnal cycle.

## ARTICLE INFO

*Article history:*
Received 24 March 2015
Received in revised form
6 July 2015
Accepted 7 July 2015
Available online 10 July 2015

*Keywords:*
Organic aerosol
Aqueous-phase dicarbonyl uptake
Anthropogenic aerosol
Biogenic aerosol
Planetary boundary layer height
Local circulation

## ABSTRACT

A field campaign combined with numerical simulations was designed to better understand the emission sources and formation processes of organic aerosols (OA) in a subtropical environment. The field campaign measured total and water soluble organic carbon (OC) in aerosol, as well as its precursor gases in the Taipei metropolis and a nearby rural forest during the summer of 2011. A regional air-quality model modified with an additional secondary organic aerosol (SOA) formation pathway was used to decipher the observed variations in OA, with focus on various formation pathways and the relative contributions from anthropogenic and biogenic sources.

According to the simulations, biogenic sources contributed to 60% and 72% of total OA production at the NTU (urban) and HL (rural) sites. The simulated fractions of SOA in total OA were 67% and 79% near the surface of NTU and HL, respectively, and these fractions increased with height and reach over 90% at the 1-km altitude. Estimated from the simulation results, aqueous-phase dicarbonyl uptake was responsible of 51% of OA production in the urban area, while the primary emissions, reversible partitioning of semi-volatile oxidation products, oligomerization of semi-volatile SOA in the particulate phase and acid-enhanced oxidation contributed to 33%, 10%, 5% and 1% respectively; in the rural area, the percentages were 59%, 21%, 13%, 7% and 1%, respectively. Meteorological factors, including large-scale wind direction, local circulation and planetary boundary layer height, all have strong influences on the source contributions and diurnal variations of OA concentration.



## 1. Introduction

Organic compounds are one of most abundant components of fine aerosol particles, particularly in areas with substantial fossil fuel and bio-fuel burning (Kanakidou et al., 2005; Zhang et al., 2007). The organic component, which we termed the organic aerosols (OA), can be classified into primary OA (POA) which are directly emitted species, and the secondary OA (SOA) which are formed by chemical reactions in the atmosphere. The fraction of SOA in total organic matter is typically 20–80% of the measured

* Corresponding author. Department of Atmospheric Sciences, National Taiwan University No. 1, Sect. 4, Roosevelt Road, Taipei, 10673, Taiwan.
*E-mail address:* jpchen@as.ntu.edu.tw (J.-P. Chen).

http://dx.doi.org/10.1016/j.atmosenv.2015.07.005
1352-2310/

mass (Carlton et al., 2009; He et al., 2011), but the values have large spatial and temporal variations. Kanakidou et al. (2005) reported that 20–50% of the total fine aerosol mass in the mid-latitudes is organics, and the fraction can be up to 90% in tropical forested areas, indicating the importance of biogenic sources in warm and humid environments.

Although field measurements may provide the spatial and temporal distributions of OA compositions, it is difficult to decipher the sources and formation processes of OA due to their complex chemical mechanisms and variation with meteorological conditions. A more comprehensive way for understanding OA production pathways is to combine the advantages of measurements and numerical models with resolved chemical and meteorological processes. Because of the complexity of precursor volatile organic compounds (VOCs) and the unclear formation pathways of SOA, including gas-to-particle conversion and heterogeneous chemistry (Gard et al., 1998; Kanakidou et al., 2005), simulating the SOA cycle using air quality models remains a challenging task (Hallquist et al., 2009). In traditional models, SOA forms via the partitioning of precursors' oxidation products onto the existing organic aerosol (Odum et al., 1996; Pankow, 1994). More recent models have considered SOA formation by in-cloud reactions (Carlton et al., 2008). However, the simulated SOA in the boundary layer and aloft usually remain underestimated (Carlton et al., 2010; Heald et al., 2011; Jathar et al., 2014), so some SOA formation processes may be missing in the models.

Taipei is a major metropolitan area surrounded by mountains covered in subtropical rainforests, so emission of SOA and its precursors are ample from both anthropogenic and natural sources. A few studies have reported measurements of carbonaceous aerosol concentrations in Taiwan. For example, Chou et al. (2010) found that POA and SOA each contributed 11 ± 6% and 18 ± 4%, respectively, of the total $PM_{2.5}$ in Taipei, according to measurements conducted in 2003–2007. However, detailed analysis of source contributions and formation processes associated with carbonaceous aerosols, particularly SOA, are scarce in this area.

To understand the impacts of human activities on the physicochemical properties of aerosols over such an urban area, a field campaign was conducted over the Taipei metropolis and an adjacent rural area in summer 2011. The US EPA Models-3/Community Multi-scale Air Quality (CMAQ) model was also applied to simulate organic aerosol formation during this field campaign to investigate its various sources and formation pathways. The model was modified following Li et al. (2013) by considering the irreversible uptake of dicarbonyls by aqueous particles as an additional pathway for SOA formation. The simulations results were evaluated by comparison with data collected during the field campaign. The discussions focus on the model performance with respect to carbonaceous compounds in the Taipei metropolis and the contributions of various sources and formation processes to OA concentrations.

## 2. Methodology

### 2.1. Measurements

The Taipei metropolis is a densely populated region with substantial anthropogenic emissions. It is located in a subtropical basin surrounded by highly vegetated mountains or highland (see Fig. 1a), and thus is a unique location for studying the complex contributions of OA from anthropogenic versus biogenic sources. For understanding the characteristics of OA in Taipei and the adjacent areas, a field campaign conducted by the Academia Sinica and National Taiwan University (hereafter referred to as NTU) was conducted during Aug. 15–21, 2011. Two contrasting measurement sites were selected, one at the urban area and the other in a rural area (see location map in Fig. 1a). The NTU campus site (25.02°N, 121.53°E; black star in Fig. 1a) is located in the southern part of the city. The sampling inlet was set up on the top floor of a building, and is approximately 25 m above ground. The HuaLin site (hereafter referred to as HL; 24.88°N, 121.56°E; yellow star in Fig. 1a) is in a rural environment, located 15 km south of NTU and 10 km away from the nearest suburban city of Sindian. At an elevation of 410 m, the HL site is surrounded by bushes and broad-leaved trees, and without significant human activities.

Simultaneous chemical measurements at NTU and HL include isoprene, $O_3$, elemental carbon (EC), and organic carbon (OC) mass concentrations, the latter two were measured with Sunset semi-continuous OC-EC Field Analyzer (Sunset OC-EC). Two sets of 12-hr-accumulation filter samples were collected daily at each site, one from 8 a.m. to 8 p.m. local time to represent daytime conditions, and the other from 8 p.m. to 8 a.m. to represent nighttime conditions. The water-soluble organic carbon (WSOC) concentration was computed as the difference between water-soluble total carbon (WSTC) and water-soluble inorganic carbon (WSIC, is the structural basis for inorganic compounds such as gas carbonates

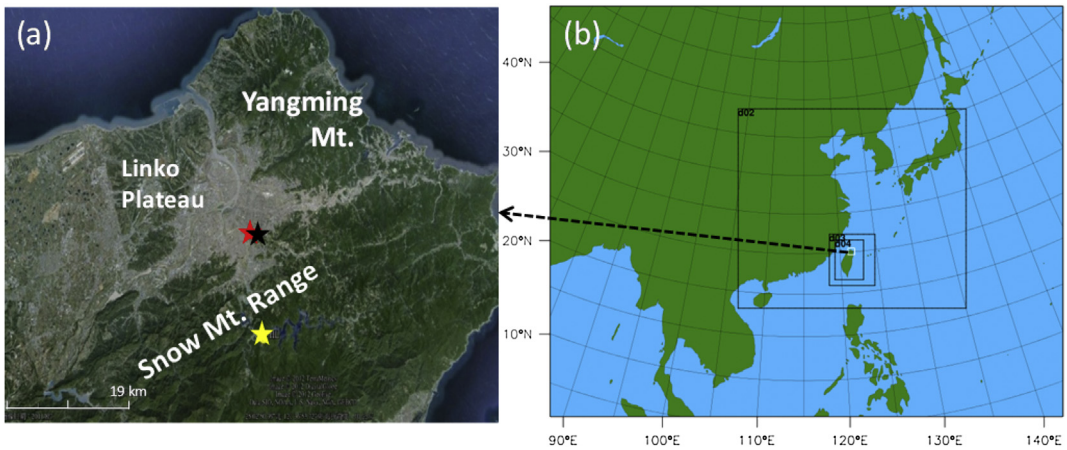


**Fig. 1.** (a) Satellite image of the Taipei metropolis (gray shading area) and its surroundings: the Yangming Mt. (peak elevation 1120 m) to the north, the Snow Mt. Range (peak elevation 3703 m) that extends from the east to the southwest, and the Linko Plateau (elevation 250 m) to the west. The locations of NTU, HL and TWEPA Guting sites are indicated by the black, yellow and red stars, respectively. (b) Geographic view of the model domains for the simulations in this study, and the white-rectangle area corresponds to the domain in (a). (For interpretation of the references to colour in this figure legend, the reader is referred to the web version of this article.)

and carbonate ions). WSTC was measured at 680°C using a total carbon analyzer (TOC-VCPH, Shimadzu Scientific Instruments), while WSIC was measured at the same temperature after adding 2 N hydrochloric acid in water (pH < 3) to the samples. The isoprene concentrations were determined using gas chromatography (Varian CP-3800) with parallel detectors (Varian Saturn 2200 ion-trap mass spectrometer and flame ionization detector; Chang et al., 2010), and the 1-h whole-air samples were collected with canisters every 2 h. The 1,3-butadiene concentration was also measured to estimate anthropogenic isoprene mixing ratio using the formula from Wang et al. (2013).

In addition to the 12-h sampling of the OC mass concentration, we also used the hourly data of OC at HL that measured with the Sunset OC-EC. The $O_3$ concentration at HL was measured with UV photometric ozone analyzer (Thermo Scientific, Model 49i). At NTU, $O_3$ was not measured locally, but represented with data from a nearby (~1.2 km away) Taiwan Environmental Protection Administration (TWEPA) station at Guting. A dual-wavelength Raman and Depolarization lidar (Chen et al., 2007; Chou et al., 2007) was used to derive the planetary boundary layer height (PBLH) at NTU with a retrieval method based on the work of Brooks (2003). The limitation of lidar retrieval is 300 m; therefore PBLH below this limit will not be reported.

### 2.2. Model

We used the CMAQ model version 4.7 (Byun and Schere, 2006) to simulate OA over East Asia with focus on the Taipei metropolitan area. Meteorological fields to drive the CMAQ simulations were obtained using the Weather Research and Forecasting (WRF) model v3.3.1 (Skamarock et al., 2008). Fig. 1b shows the four nested domains for our CMAQ simulations, with horizontal resolutions of 81, 27, 9, and 3 km. The vertical dimension includes 28 layers (surface to 50 hPa), 8 of which are assigned to heights below 1.5 km to emphasize boundary layer processes. The initial and boundary conditions for the meteorological fields were obtained from the National Centers for Environmental Prediction (NCEP) Final Global analysis (FNL) data. Wind, temperature and water vapor in the FNL data were nudged into domains 1 and 2 every 6 h.

During the one-week experiment on Aug. 15–21, 2011, Taiwan's weather was dominated by the Pacific subtropical high pressure ridge. In the early half of the week (Stage 1), the large-scale wind around Taipei was from the south (Fig. 2). In the latter half of the week (Stage 2), the large-scale wind became weaker and turned easterly as the Pacific high pressure ridge shifted northward. The simulation results shown in Fig. 2 indicate that the WRF model can reproduce quite well the synoptic-scale patterns and changes in wind directions over Taiwan from Stage 1 to Stage 2. As will be discussed in more details, such a change in large-scale wind direction has strong influences on the transport of aerosol particles and their precursors.

Anthropogenic emissions of POA, VOC precursors, and other major primary pollutants over East Asia were taken from the emission inventory of Zhang et al. (2009) and were interpolated to

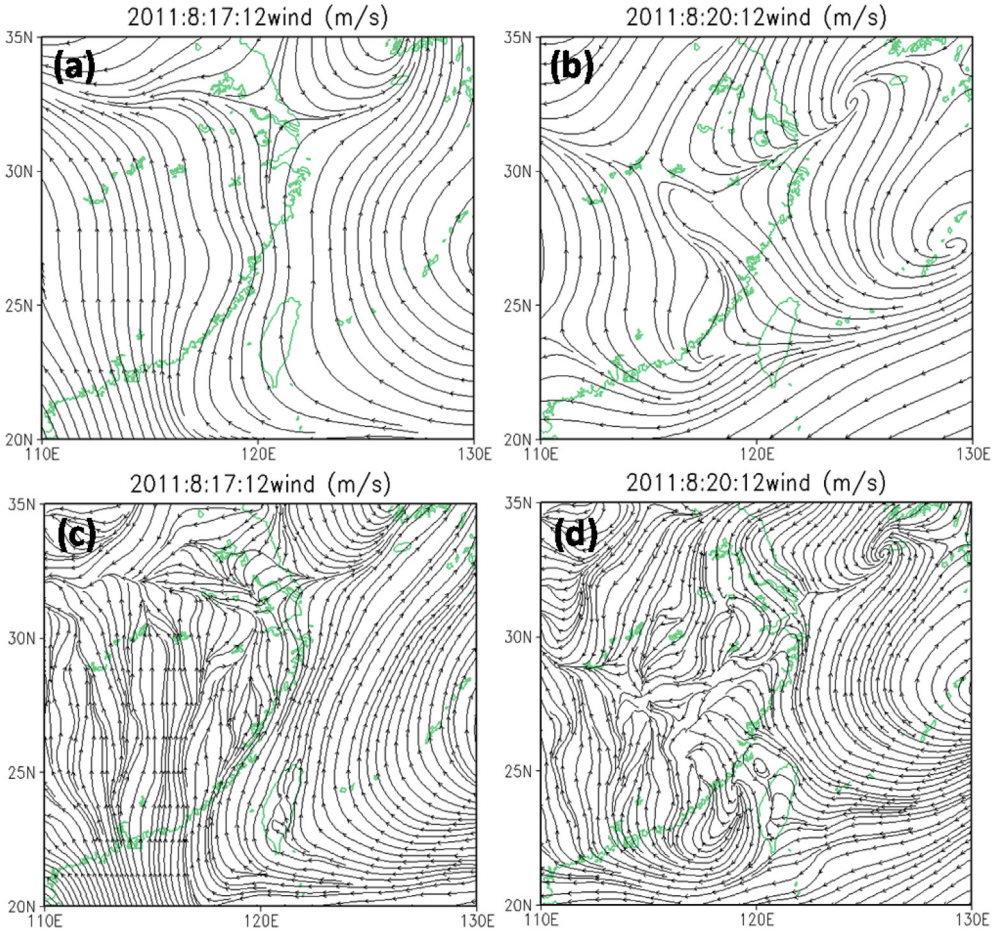


**Fig. 2.** Wind streamlines from NCEP reanalysis data (top) and WRF domain 2 simulation (bottom) at 12Z Aug. 17 (left) and 12Z Aug. 20 (right). Difference in streamline density between the NCEP data and WRF results is due to different data resolution (1° × 1° for the reanalysis data and 27 km × 27 km for WRF).

**Table 1**
The OA/OC mass ratio for different SOA species based on Kleindienst et al. (2007).

| Species | OA/OC ratio |
|---|---|
| Semivolatile SOA formation from benzene, low-yield aromatic and high-yield aromatics | 2 |
| Nonvolatile SOA formation from benzene, glyoxal, methylglyoxal, low-yield aromatic and high-yield aromatics | |
| Semivolatile SOA formation from sesquiterpenes | 2.1 |
| Nonvolatile aged aerosol | |
| Nonvolatile SOA formation from isoprene (acid enhancement) | 2.7 |
| Semivolatile SOA formation from isoprene | 1.6 |
| Semivolatile SOA formation from long alkanes | 1.56 |
| Semivolatile SOA formation from monoterpenes | 1.4 |

our model grids from its resolution of 0.5° × 0.5°. Over Taiwan, we applied the 1-km resolution anthropogenic emission inventory from the Taiwan Emission Data System version 7.1 (http://ivy2.epa.gov.tw/air-ei) developed by the TWEPA. Biogenic VOC emissions were calculated with the Model of Emission of Gases and Aerosols from Nature algorithm (MEGAN, version 2.04) (Guenther et al., 2006) with land cover and leaf area index data from the NASA MODIS satellite instrument (https://lpdaac.usgs.gov/). Biomass burning emission is not significant around Taipei, so it was not included in the simulation.

The gas-phase chemistry mechanism used in this study is SAPRC-99 (Carter, 2000; Carlton et al., 2010). Four different pathways for SOA production were included in our model: (1) semivolatile SOA produced via the reversible partitioning of semivolatile oxidation products of isoprene, monoterpenes, sesquiterpenes, aromatics, and long alkanes; (2) non-volatile SOA produced via oligomerization of semi-volatile SOA in the particulate phase; (3) non-volatile SOA produced via acid-enhanced oxidation of isoprene and aromatics (low-NOx); and (4) non-volatile SOA produced via the irreversible aqueous uptake of dicarbonyls (glyoxal and methylglyoxal) by wet aerosols and cloud/fog droplets. The first three pathways were from Carlton et al. (2010). The fourth pathway was implemented into CMAQ following Li et al. (2013), largely supported by two upgraded modules: (1) more detailed gas-phase chemistry of dicarbonyls (Fu et al., 2008), and (2) aqueous uptake of dicarbonyls with a reactive uptake coefficient of $2.9 \times 10^{-3}$ (Liggio et al., 2005; Zhao et al., 2006). It has been verified with observations over eastern North America (Fu et al., 2009) and the Pearl River Delta region (Li et al., 2013).

Three simulations were performed to understand the relative contributions of SOA formation from anthropogenic versus biogenic VOC precursors and the aqueous-phase reactive production. The control run (CTRL) included both anthropogenic and biogenic emissions, as well as the additional aqueous-phase dicarbonyl reactions using updated SAPRC99; the anthropogenic run (ANTH) excluded the biogenic emissions, whereas the no dicarbonyl run (NO_DICA) excluded the aqueous-phase dicarbonyl pathway. All simulations were performed for the period of August 4–21, 2011, but only results that corresponded to the field measurement period (i.e., August 15–21) were analyzed. The organic-to-carbon mass ratios (OA/OC) used for model result analysis were adopted from Kleindienst et al. (2007), as listed in Table 1.

## 3. Sources of isoprene in the Taipei metropolis

Isoprene is thought to be one of the major precursors of SOA due to its large global emissions and high reactivity, and has strong contributions from both anthropogenic and biogenic sources (Claeys et al., 2004; Hallquist et al., 2009). Fig. 3a–b compares the observed and simulated isoprene concentrations at NTU and HL. The observed isoprene generally reached its peak at noon and decreased to a rather low value at night. The daily maximum concentrations ranged from 1.5 to 2.7 ppb at NTU and 1.5 to 2.5 ppb at HL. Compared with observations, the simulated isoprene was

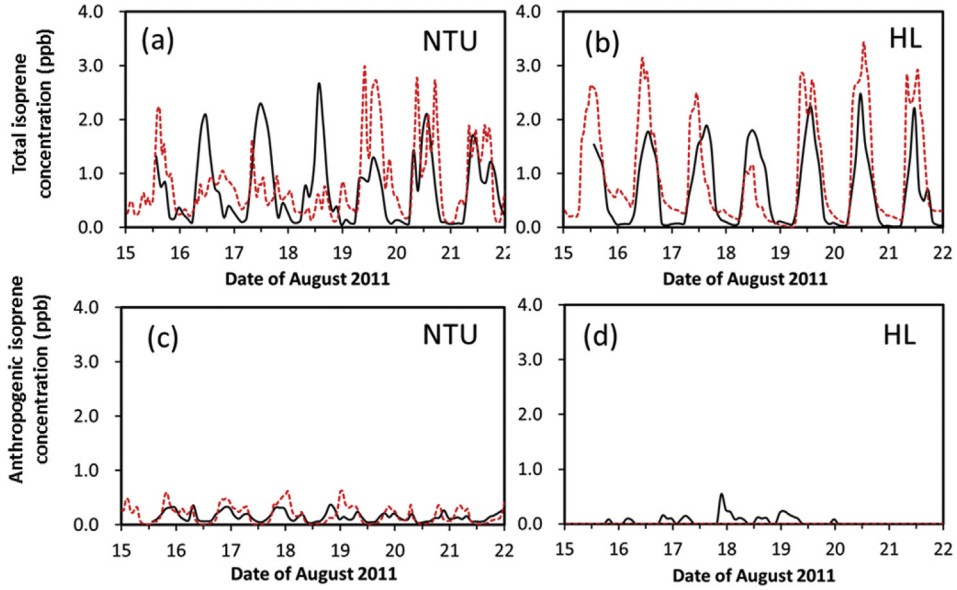


**Fig. 3.** Evolution of total (upper panels) and anthropogenic (lower panels) isoprene concentrations. Left and right panels were at NTU and HL, respectively. Observed values are in black lines, whereas the simulated values are in red-dashed lines. (For interpretation of the references to colour in this figure legend, the reader is referred to the web version of this article.)

somewhat underestimated during Stage 1 and overestimated during Stage 2 at NTU. The simulation at HL agreed better with the observations in terms of the diurnal cycle and peak values, although the peak values were slightly overestimated.

The anthropogenic isoprene (estimated from the 1,3-butadiene measurement) at NTU generally showed two peaks, one during the morning and the other in the evening rush hours, and the latter peak sometimes extended toward midnight (Fig. 3c). The diurnal double-peak feature were accentuated in the model results, with values underestimated during daytime and overestimated during nighttime. At HL, the anthropogenic isoprene concentration was often below the detection limit, especially during Stage 2, whereas the simulated values are always close to zero (Fig. 3d).

SOA formation is closely related to photochemical reactions, so the simulated $O_3$ concentrations were briefly examined to assess the model's performance in photochemistry. As shown in Fig. 4, the simulated $O_3$ concentration at Guting was quite comparable to the observations, with the highest peak of 125 ppb occurred during the transition of southerly to southeasterly winds (i.e., on Aug. 18th). At HL, although some breaks exist in the observational data, the model was able to capture the $O_3$ variation patterns well. The overall agreement in simulated $O_3$ with observations indicated our model's capability in calculating photochemistry and thus SOA formation processes that will be discussed next.

## 4. OA sources and formation pathways

The sources of OA include POA and formation from precursors, and it is difficult to differentiate these sources according to observations. Thus, we rely on model simulations to evaluate various sources and production pathways. The simulated OC was compared with the 12-h sampling of OC concentrations at NTU and HL (Fig. 5a–b). The observed OC varied between 2 and 9 $\mu g/m^3$ at NTU, and a similar variation was found at HL. In Stage 1, the mean OC concentration was above 5 $\mu g/m^3$, with no obvious diurnal patterns. In Stage 2, the OC concentration became significantly lower, and the diurnal variation became obvious. Because WSOC tends to highly correlate with SOC in the measurements (Miyazaki et al., 2006), we evaluated the simulated SOC with observed WSOC concentration in Fig. 5c–d. Over all, the simulated OC was lower than that observed, but the simulated SOC is rather similar to the observed WSOC in terms of the magnitude and diurnal patterns at both sites.

Fig. 6a showed the spatial pattern of OA's biogenic fraction. It was low over the northwestern side of Taipei metropolis, especially the downtown area (<20%), but increased toward the rural areas especially the Snow Mt. Range (SMR) over the south (>80%). Table 2 shows that the simulated biogenic fractions of isoprene were 69–82% at NTU and near 100% at HL. These fractions are quite close to those observed during Stage 2 at both NTU and HL, but are somewhat lower (higher) than observed during stage 1 at NTU (HL). The discrepancies are related to errors in emission and transport process which will be further elaborated. The simulated biogenic fractions of SOA, on the other hand, are all around 90%, which are higher (lower) than the biogenic fractions of isoprene at NTU (HL). This reflects mainly the transport effect, because the biogenic fraction of SOA at NTU can increase under stronger winds which bring in biogenic SOA from the surrounding mountains. In contrast, at HL the transport from the urban areas tends to reduce the fraction of biogenic SOA. But such a transport effect is much less obvious for isoprene due to its shorter lifetime. Another cause for the discrepancies between the simulated biogenic fractions of isoprene and SOA is the extra (but minor) sources of SOA from other biogenic precursors such as monoterpene. The biogenic fraction of total OA is even lower, as can be seen from Table 2. This is mainly due to the extra contribution from POA. The fraction of POA in total OA at NTU is about 33%, and one can calculate from this that a 90% biogenic fraction in SOA will convert to a 60% in OA. The latter value is rather close to the 60–61% given in Table 2.

Fig. 6b showed the fraction of OA produced from aqueous-phase reactions, and its geographic distribution is somewhat dissimilar to that of biogenic OA fraction shown in Fig. 6a. The lowest values still occurred at the downwind metropolis, but the highest values occurred over the southern mountains and the oceans. These contrasts indicated that aqueous-phase productions were strongly associated with aerosol water content and thus the relative humidity, which tended to be high in the mountains and over the oceans.

To understand the relative importance of the contribution pathways, the OA concentrations from POA and SOA for four pathways were analyzed in Fig. 7. During Stages 1–2, POA contributed 33% of OA at NTU and 21% at HL. Aqueous phase reactions (SOA_P4 in Fig. 7) is the most important pathway, contributing 51% of the OA at NTU and 59% at HL. The "reversible partitioning of semi-volatile oxidation products (SOA_P1 in Fig. 7)", "oligomerization of semi-volatile SOA in the particulate phase (SOA_P2 in Fig. 7)" and "acid-enhanced oxidation (SOA_P3 in Fig. 7)" each contributed 10%, 5% and 1%, respectively, at NTU; whereas the percentages were 13%, 7% and 1%, respectively, at HL.

In addition to horizontal geographic variations, the OA concentration and SOA fraction also varied significantly with height as shown in Fig. 8. The SOA fraction increased with height because air temperature in a well-mixed boundary layer usually decreased with altitude. This caused the relative humidity to increase with height, allowing aerosol particles to absorb more water and even form clouds near the boundary layer top. Therefore, a stronger aqueous-phase production of SOA occurred aloft, and the fraction of SOA in total OA increased from 67% to 92% from the surface to the 1-km height at NTU and from 79% to 94% at HL.

## 5. Influence of meteorological fields on OA distribution

Atmospheric circulation played an important role in the spatial

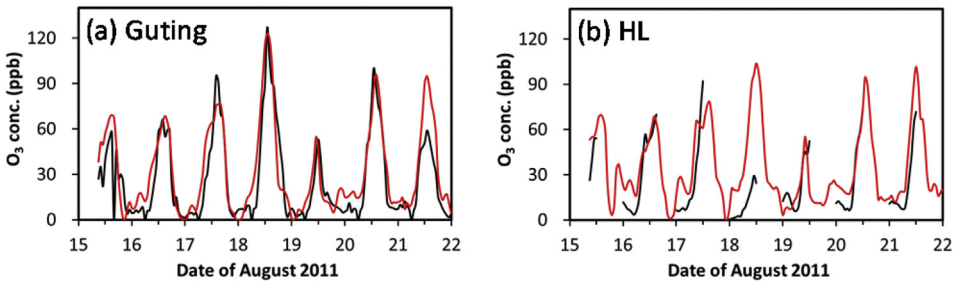


**Fig. 4.** Comparisons between observed (black line) and simulated (red line) $O_3$ concentrations at (a) Guting and (b) HL.(For interpretation of the references to colour in this figure legend, the reader is referred to the web version of this article.)

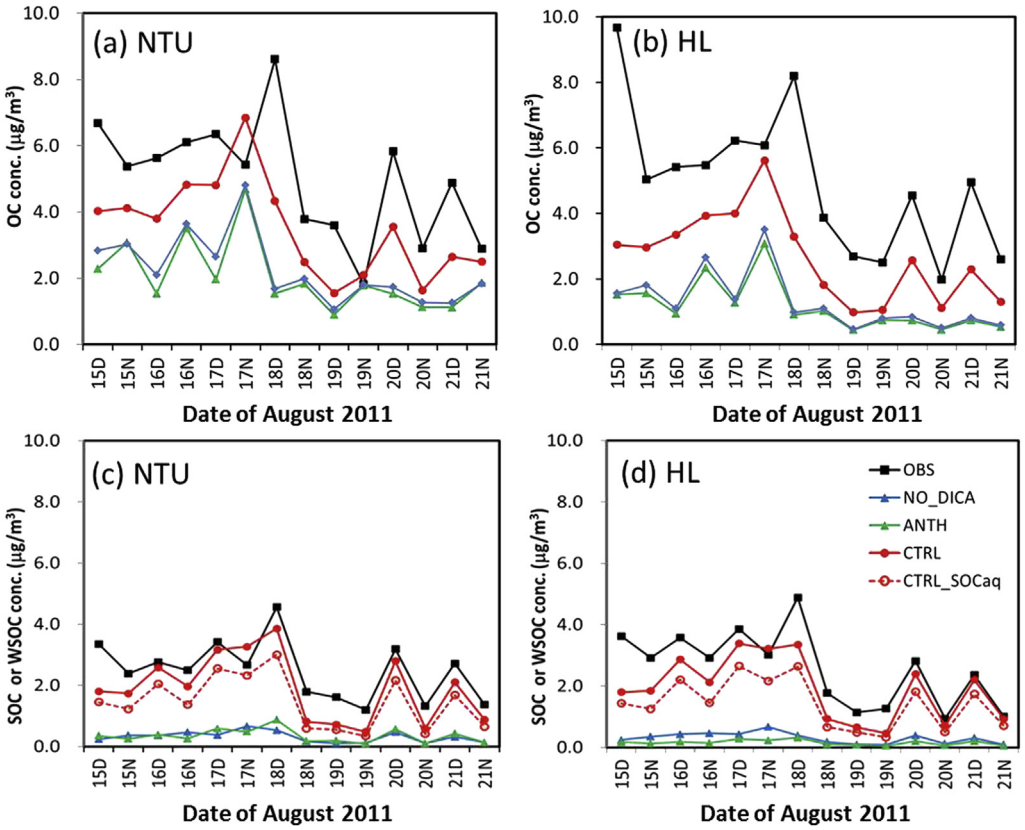


**Fig. 5.** Comparisons between observed (black lines) and simulated OC (top), and between observed WSOC and simulated SOC (bottom) at the NTU and HL. The results from the CTRL run, ANTH run and NO_DICA run are in red, green and blue lines, respectively. The red dashed lines (CTRL_SOCaq) refers to SOC formed from aqueous reactions. In the abscissa labels, "D" indicates daytime (8 a.m.–8 p.m.) and "N" indicates nighttime (8 p.m.–8 a.m.). (For interpretation of the references to colour in this figure legend, the reader is referred to the web version of this article.)

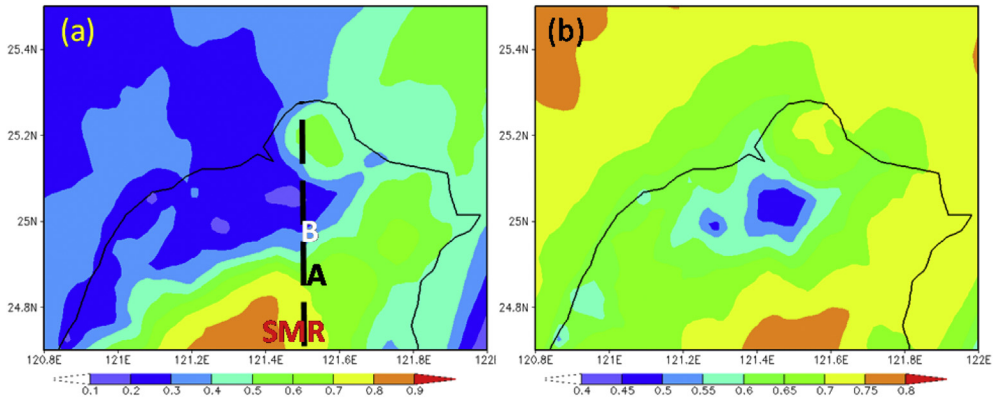


**Fig. 6.** Simulated fractions of (a) biogenic OA, and (b) aqueous-phase SOA to the total OA productions over the inner domain. The values were averages during Aug. 15–21, 2011. The vertical dashed line at 121.53°E in (a) indicated the cross-section range shown in Fig. 9. Markers "SMR", "A", and "B" indicate the Snow Mt. Range, HL and NTU.

**Table 2**
Mean values of observed isoprene, WSOC and OC, as well as simulated isoprene, SOA and OA concentrations. Values shown in the brackets are the biogenic fractions.

| | | NTU | | HL | |
|---|---|---|---|---|---|
| | | Stage 1 | Stage 2 | Stage 1 | Stage 2 |
| Observation | Isoprene, ppb | 0.73 (77%) | 0.74 (83%) | 0.72 (80%) | 0.61 (100%) |
| | WSOC, μg/m$^3$ | 2.78 | 1.96 | 3.08 | 1.68 |
| | OC, μg/m$^3$ | 5.73 | 3.66 | 5.85 | 3.32 |
| Simulation | Isoprene, ppb | 0.63 (69%) | 0.99 (82%) | 0.96 (100%) | 1.13 (100%) |
| | SOA, μg/m$^3$ | 4.43 (91%) | 2.74 (90%) | 4.49 (92%) | 2.68 (91%) |
| | OA, μg/m$^3$ | 6.65 (61%) | 4.08 (60%) | 5.79 (71%) | 3.21 (77%) |

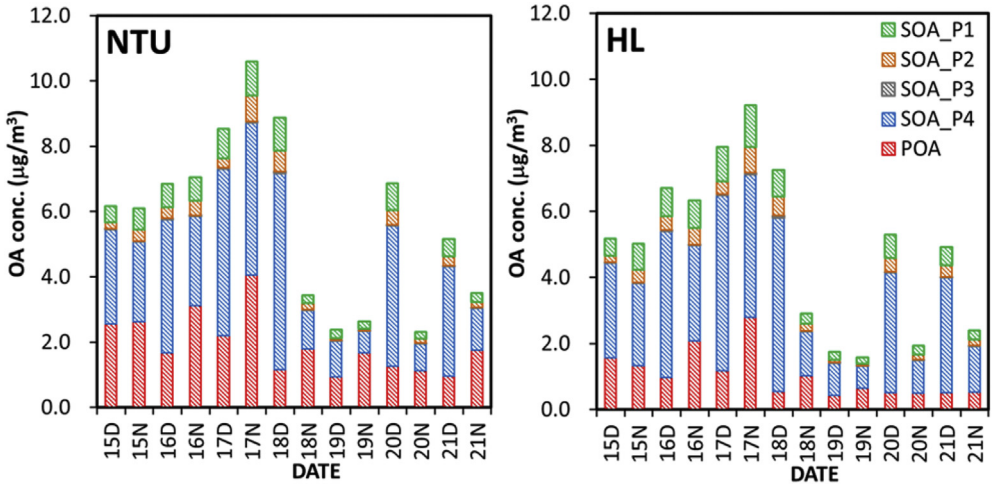


**Fig. 7.** Concentration of simulated OA from CTRL run at NTU (left) and HL (right). The formation pathways including SOA_P1 (green bar), SOA_P2 (orange bar), SOA_P3 (gray bar), and SOA_P4 (blue bar) were described in the text. (For interpretation of the references to colour in this figure legend, the reader is referred to the web version of this article.)

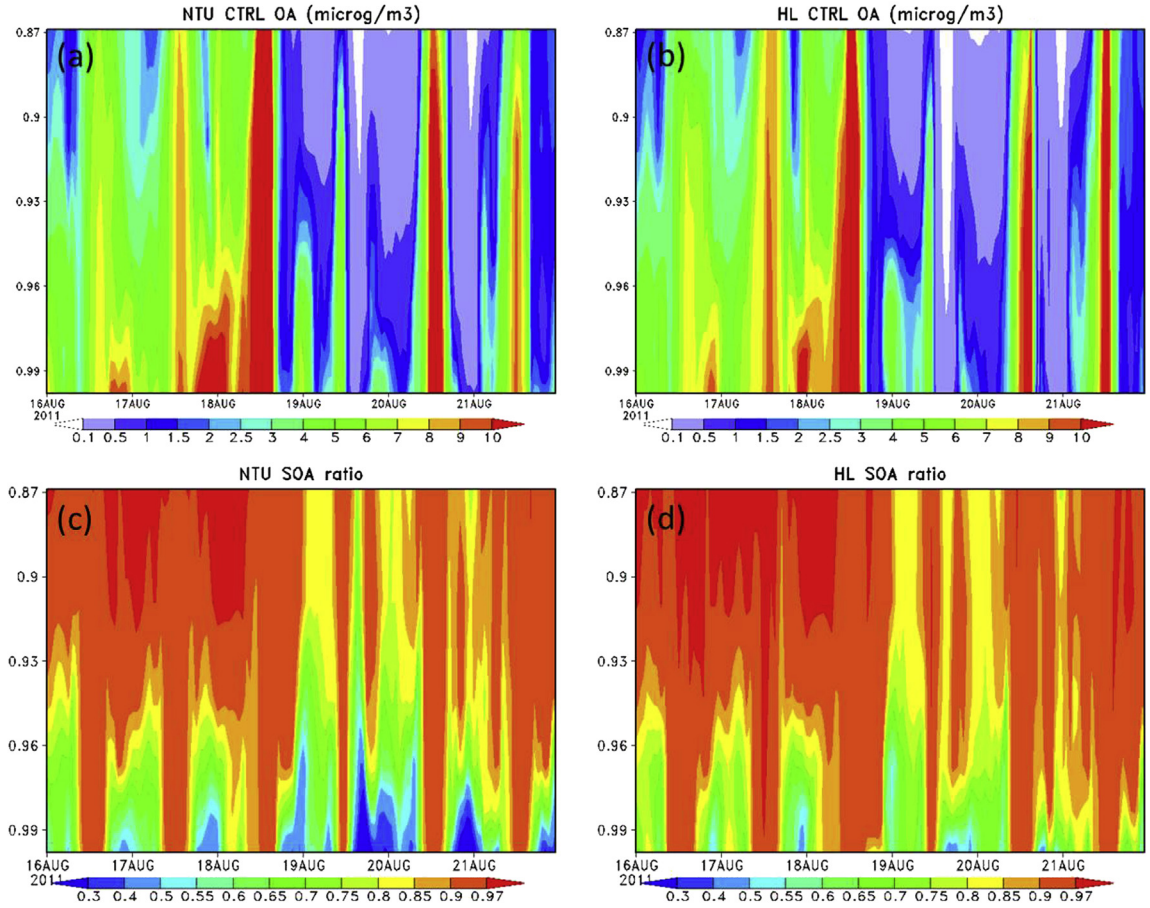


**Fig. 8.** Simulated vertical distribution of total OA concentration (top, μg/m$^3$) and the SOA fraction to the total OA (bottom) at NTU (left) and HL (right). The ordinate is sigma value of the vertical layer in the model; for example, 0.9 roughly corresponds to the 900 hPa level or 1 km altitude.

distribution of OA as shown by the time-latitude Hovmöller diagram in Fig. 9a. Because of the north-south orientation of Taiwan's main mountain range, air reaching Taipei tends to have stayed longer in the mountains when traveling from the south than from the east. So, a switch from the southerly winds (Stage 1) to easterly winds (Stage 2) would lead to lower OA concentrations as well as biogenic OA fractions over Taipei and even the SMR (see Fig. 9b). This also means that the eastern mountains are under stronger influence of the oceans such that the biogenic OA over there was significantly lower than over the southern mountains.

Without a strong transport of biogenic OA from the south, the diurnal pattern in biogenic OA fraction became much more

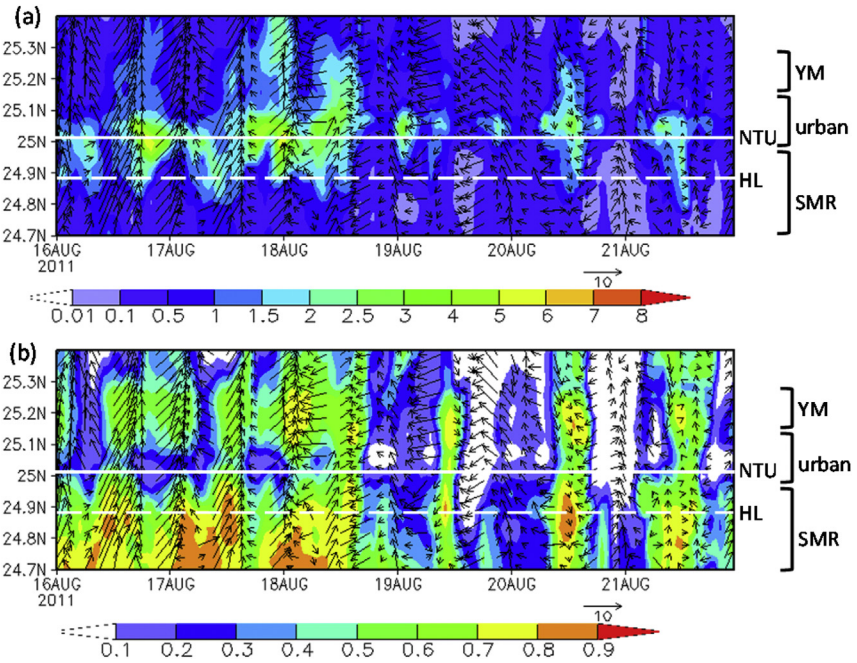


**Fig. 9.** Temporal evolution of (a) the total OC concentration (μg/m$^3$) and (b) the biogenic OC fraction in total OC at the north-south cross section at 121.53°E between latitudes 24.7°N and 25.4°N (see Fig. 6a for the geographic location). Also overlaid were surface wind vectors given in a 3-h interval. Labeled on the right were the latitudinal locations of NTU and HL, as well as the locations of the urban area, Yangming Mt. (YM) and Snow Mt. Range (SMR).

prominent during Stage 2. This also caused the noontime peak in OA's biogenic fraction near the Yangming Mt. (around 25.2°N in Fig. 5b) to become more prominent than during Stage 1. Note that the southerly wind did not seem to replenish isoprene at NTU, which was still underestimated during Stage 1 as discussed earlier. As isoprene has a short lifetime of approximately 2 h, it is likely that they were largely converted into OA before arriving NTU.

Not only the large-scale winds but also the local circulation can influence the OA concentrations. As shown in Fig. 9, the local circulation during Stage 1 was manifested by the switch of wind direction from southwest around mid-night to southeast before dawn, and then switched back to southwest around noon. That occurred again during the afternoon (southwest winds) and into the evening (southeast winds). This diurnal pattern tends to bring the OA particles back and forth over the Taipei basin and surrounding mountains, resulting in dual daily peaks in the biogenic OA fraction as shown in Fig. 9b. Another interesting feature is the low biogenic OA fraction over the Yangming Mt. in the early morning during Stage 1. This anthropogenic influence occurred when the wind was straight from the south and thus the urban center sits directly upwind of the Yangming Mt. The double-peak phenomenon largely disappeared during Stage 2 because of changes in the large-scale winds and the local wind pattern.

These results showed that the complexity of OA sources cannot be fully resolved without understanding the transport effects from the large-scale wind and local circulation combined. Wet deposition is another important factor concerning aerosol transportation, but it is not relevant to this study because no significant precipitation occurred during this field campaign.

## 6. Discussion

Although the CTRL run adequately reproduced the OA distribution in the Taipei metropolis, discrepancies still exist between the model and observations. In contrast to the good relationship between the simulated SOC and the observed WSOC concentration (Fig. 5c–d), the variations in the simulated OC concentrations were not well-correlated with the observed OC concentrations (Fig. 5a–b), particularly during Stage 1. We focused on SOC to discuss whether the discrepancy in the simulated OC was of primary or secondary origin. If a WSOC to SOC ratios of 0.7 (cf. Miyazaki et al., 2006) was applied, the WSOC that derived from simulated SOC would be within a factor of 2 of observed WSOC. If this could be used to indicate that the production of SOA was reasonably well simulated, then the underestimation in OC should come mainly from errors in primary emissions. Such an assertion may be supported by the deficits in simulated EC, which was exclusively of primary origin, as shown in Fig. 10. Note that POA emissions may be underestimated in not only Taiwan but also the whole East Asia region, as reported by Fu et al. (2012) and Cohen and Wang (2014).

Fig. 5a–b and Fig. 10 also revealed another discrepancy, as the simulated nighttime EC and OC concentrations were higher than in daytime during Stage 1. In the Taipei metropolis, the daytime POA emission rates were higher than the nighttime rates in the inventory, with two peaks occurring during the rush hours (6–9 a.m. and 4–8 p.m.). Therefore, the nighttime high concentrations from the model during Stage 1 may be due to meteorological conditions. Fig. 11 showed that PBLH retrieved from the lidar measurement at NTU peaked around noon, with maxima ranging from 800 to 1500 m; it then decreased in the afternoon and lowered to below 400 m before dawn. The simulated PBLH fitted the morning increase rather well, yet it dropped off too quickly in the afternoon and continued to underestimate it at night during Stage 1. As pollutants tend to be trapped in the PBL, too shallow PBL may result in overestimated pollutant concentrations. A sensitivity test was performed by imposing the observed PBLH at NTU, and it showed that the nighttime EC at NTU indeed decreased significantly, while the daytime EC remained relatively unchanged. But the simulated nighttime EC concentrations were still higher than during daytime, possibly due to transport from unadjusted neighboring grids. The PBLH was better simulated during Stage 2, and this was also when

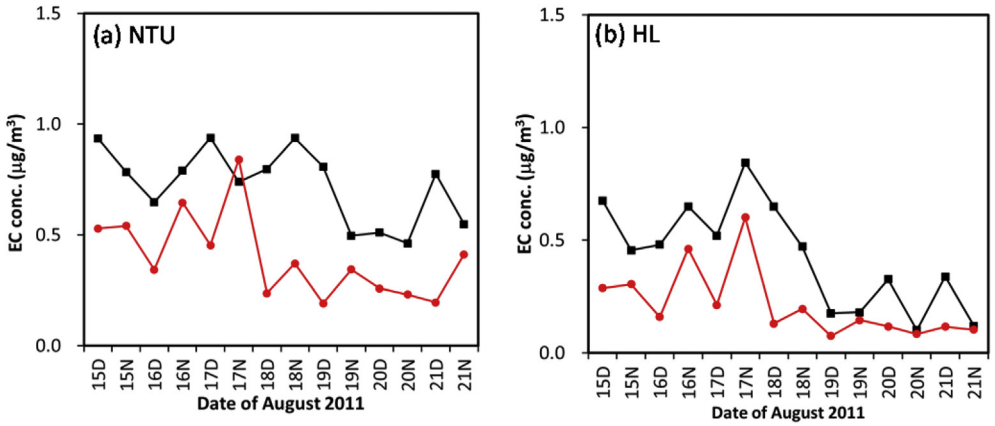


**Fig. 10.** Comparison between observed (black line) and simulated (CTRL run, red line) EC mass concentrations at the (a) NTU and (b) HL. (For interpretation of the references to colour in this figure legend, the reader is referred to the web version of this article.)

the simulation did not overestimate the nighttime EC and OC concentrations.

In addition to the primary emissions and meteorological fields, uncertainties might also have been introduced by the assumptions used in this study. First, we assumed that all SOC were soluble when comparing with the observed WSOC (red solid lines in Fig. 5c–d). Our simulations would have larger deficits in SOC production if some of the SOC is insoluble. For example, assuming soluble SOC can only be produced from aqueous reactions (red dashed lines in Fig. 4c–d), then the simulated SOC would be about 45% lower than observed WSOC (even though their time variations correlated rather well).

A second uncertainty may be in the omission of evaporation of semivolatile POA. Recent studies found that the aging of semivolatile and intermediate volatility organic compounds (S/IVOC) that released from POA to the air may be important sources of SOA (Robinson et al., 2007) after that fraction reacts in the gas phase. If this potential source of anthropogenic SOA was included, the biogenic OA contribution could be lower than 40% at NTU. Matsui et al. (2014) pointed that the aging process of S/IVOC could effectively improve the model performance of SOA simulation and enhance the interaction of anthropogenic and biogenic sources.

The irreversible uptake of dicarbonyl SOA is another source of uncertainty. By considering the additional dicarbonyl processes, the SOC concentrations were increased (blue line in Fig. 5c–d), and the correlation between hourly observed and simulated OC increased from 0.36 to 0.73 at HL (Fig. 12). However, Galloway et al. (2009) reported that glyoxal oligomers formation through acid catalyzed pathways was actually reversible. This suggested that the aqueous-phase SOA formation may be overestimated in this study. So, the chemical mechanisms of SOA formation apparently still needs further understanding.

## 7. Conclusions

From the results of field campaign and numerical simulations, we estimated the sources and formation processes of OA in the Taipei metropolis and its surrounding subtropical forest in the summer of 2011. Observation and simulation results indicated that about 70–80% of the isoprene were from biogenic sources at NTU.

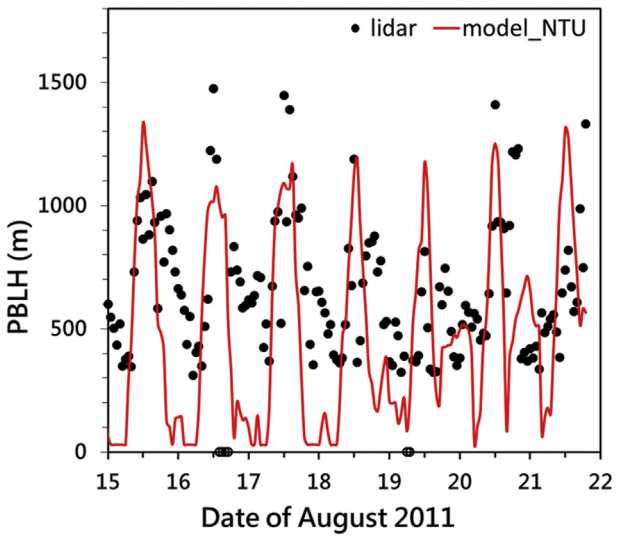


**Fig. 11.** Comparison between lidar-retrieved PBLH (black dot) and simulated PBLH at NTU (red line). PBLH that were below the 300 m retrieval or missing data are marked as hollow circles on the baseline. (For interpretation of the references to colour in this figure legend, the reader is referred to the web version of this article.)

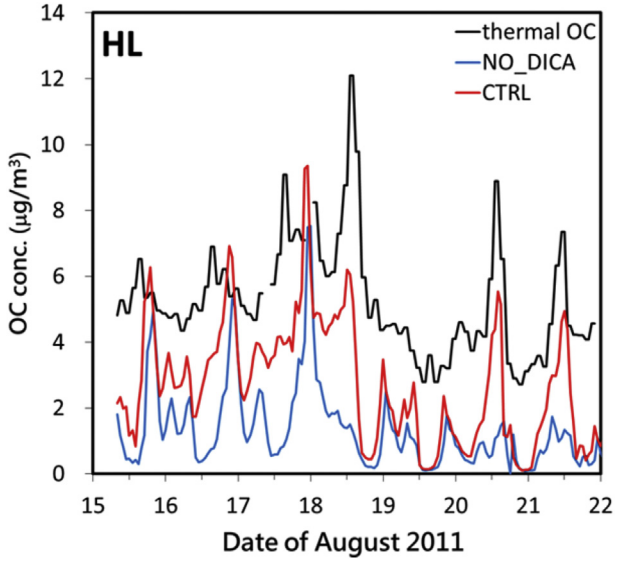


**Fig. 12.** Hourly observed OC (black line) and simulated OC in the NO_DICA (blue line) and CTRL (red line) runs at the HL. (For interpretation of the references to colour in this figure legend, the reader is referred to the web version of this article.)

Simulations showed that biogenic sources contributed 60% of the OA production at NTU and 72% at HL. The biogenic contribution to SOA is even higher, with 91% at NTU and 92% at HL.

The aqueous-phase pathway turned out to be very important, contributed 51% of the OA mass in the urban area, while 33%, 10%, 5% and 1% of the OA were from the POA, SOA_P1, SOA_P2 and SOA_P3, respectively. Over the rural area, the percentages were 59%, 21%, 13%, 7% and 1%, respectively. Simulation results showed that the fractions of SOA in total OA were 67 and 79% near the surface of NTU and HL, respectively, and these fractions increased with height and can reach well over 90% at the 1-km altitude.

Supported by observations, model results showed that the fraction of biogenic OA was higher in the southern part of the Taipei city, including HL and NTU when the large-scale wind direction was from the SMR to the south during Stage 1. But when the large-scale wind shifted to easterly during Stage 2, transport from the southern mountains diminished, leading to lower concentration in the southern metropolis. Other meteorological factors, such as local circulation and PBLH also influence the concentration and diurnal variation of OA.

The model underestimated primary emissions and the secondary productions by approximately 30–40%. Although such discrepancies can be considered relatively low comparing with many earlier modeling results, there is still plenty of room for improvement in OA simulation, such as inaccurate emission inventory, missing chemical mechanisms for SOA formation, and imperfect meteorological fields.

## Acknowledgment

We would like to thank NASA Data Distribution and Archive Center for processing and providing MODIS AOD products. This study was supported by the Ministry of Science and Technology of the Republic of China in Taiwan through projects NSC-99-2111-M-002-009-MY3 and NSC-102-2111-M-002-007-MY3. All data used in this study will be available upon request to the authors.

## References

Brooks, I.M., 2003. Finding boundary layer top: application of a wavelet covariance transform to lidar backscatter profiles. J. Atmos. Ocean. Technol. 20 (8), 1092–1105.
Byun, D., Schere, K.L., 2006. Review of the governing equations, computational algorithms, and other components of the Models-3 Community Multiscale Air Quality (CMAQ) modeling system. Appl. Mech. Rev. 59 (2), 51–77.
Carlton, A., Wiedinmyer, C., Kroll, J., 2009. A review of Secondary Organic Aerosol (SOA) formation from isoprene. Atmos. Chem. Phys. 9 (14), 4987–5005.
Carlton, A.G., Bhave, P.V., Napelenok, S.L., Edney, E.O., Sarwar, G., Pinder, R.W., Pouliot, G.A., Houyoux, M., 2010. Model representation of secondary organic aerosol in CMAQv4.7. Environ. Sci. Technol. 44 (22), 8553–8560.
Carlton, A.G., Turpin, B.J., Altieri, K.E., Seitzinger, S.P., Mathur, R., Roselle, S.J., Weber, R.J., 2008. CMAQ model performance enhanced when in-cloud secondary organic aerosol is included: comparisons of organic carbon predictions with measurements. Environ. Sci. Technol. 42 (23), 8798–8802.
Carter, W.P.L., 2000. Implementation of the SAPRC-99 Chemical Mechanism into the Models-3 Framework. U. S. Environmental Protection Agency, Research Triangle Park, NC.
Chang, C.-C., OuYang, C.-F., Wang, C.-H., Chiang, S.-W., Wang, J.-L., 2010. Validation of in-situ measurements of volatile organic compounds through flask sampling and gas chromatography/mass spectrometry analysis. Atmos. Environ. 44 (10), 1301–1307.
Chen, W.-N., Tsai, F.-J., Chou, C.C.-K., Chang, S.-Y., Chen, Y.-W., Chen, J.-P., 2007. Optical properties of Asian dusts in the free atmosphere measured by Raman lidar at Taipei, Taiwan. Atmos. Environ. 41 (36), 7698–7714.
Chou, C.C.-K., Lee, C.-T., Chen, W.-N., Chang, S.-Y., Chen, T.-K., Lin, C.-Y., Chen, J.-P., 2007. Lidar observations of the diurnal variations in the depth of urban mixing layer: a case study on the air quality deterioration in Taipei, Taiwan. Sci. Total Environ. 374 (1), 156–166.
Chou, C.C.K., et al., 2010. Seasonal variation and spatial distribution of carbonaceous aerosols in Taiwan. Atmos. Chem. Phys. 10 (19), 9563–9578.
Claeys, M., Graham, B., Vas, G., Wang, W., Vermeylen, R., Pashynska, V., Cafmeyer, J., Guyon, P., Andreae, M.O., Artaxo, P., Maenhaut, W., 2004. Formation of secondary organic aerosols through photooxidation of isoprene. Science 303, 1173–1176.
Cohen, J.B., Wang, C., 2014. Estimating global black carbon emissions using a top-down Kalman Filter approach. J. Geophys. Res. Atmos. 119 (1), 2013JD019912.
Fu, T.-M., Jacob, D.J., Heald, C.L., 2009. Aqueous-phase reactive uptake of dicarbonyls as a source of organic aerosol over eastern North America. Atmos. Environ. 43 (10), 1814–1822.
Fu, T.-M., Jacob, D.J., Wittrock, F., Burrows, J.P., Vrekoussis, M., Henze, D.K., 2008. Global budgets of atmospheric glyoxal and methylglyoxal, and implications for formation of secondary organic aerosols. J. Geophys. Res. Atmos. 113 (D15), D15303.
Fu, T.M., et al., 2012. Carbonaceous aerosols in China: top-down constraints on primary sources and estimation of secondary contribution. Atmos. Chem. Phys. 12 (5), 2725–2746.
Galloway, M.M., Chhabra, P.S., Chan, A.W.H., Surratt, J.D., Flagan, R.C., Seinfeld, J.H., Keutsch, F.N., 2009. Glyoxal uptake on ammonium sulphate seed aerosol: reaction products and reversibility of uptake under dark and irradiated conditions. Atmos. Chem. Phys. 9 (10), 3331–3345.
Gard, E.E., et al., 1998. Direct observation of heterogeneous chemistry in the atmosphere. Science 279 (5354), 1184–1187.
Guenther, A., Karl, T., Harley, P., Wiedinmyer, C., Palmer, P.I., Geron, C., 2006. Estimates of global terrestrial isoprene emissions using MEGAN (Model of Emissions of Gases and Aerosols from Nature). Atmos. Chem. Phys. 6 (11), 3181–3210.
Hallquist, M., et al., 2009. The formation, properties and impact of secondary organic aerosol: current and emerging issues. Atmos. Chem. Phys. 9 (14), 5155–5236.
He, M., Zheng, J., Yin, S., Zhang, Y., 2011. Trends, temporal and spatial characteristics, and uncertainties in biomass burning emissions in the Pearl River Delta, China. Atmos. Environ. 45 (24), 4051–4059.
Heald, C.L., et al., 2011. Exploring the vertical profile of atmospheric organic aerosol: comparing 17 aircraft field campaigns with a global model. Atmos. Chem. Phys. 11 (24), 12673–12696.
Jathar, S.H., Gordon, T.D., Hennigan, C.J., Pye, H.O.T., Pouliot, G., Adams, P.J., Donahue, N.M., Robinson, A.L., 2014. Unspeciated organic emissions from combustion sources and their influence on the secondary organic aerosol budget in the United States. Proc. Natl. Acad. Sci. 111 (29), 10473–10478.
Kanakidou, M., et al., 2005. Organic aerosol and global climate modelling: a review. Atmos. Chem. Phys. 5 (4), 1053–1123.
Kleindienst, T.E., Jaoui, M., Lewandowski, M., Offenberg, J.H., Lewis, C.W., Bhave, P.V., Edney, E.O., 2007. Estimates of the contributions of biogenic and anthropogenic hydrocarbons to secondary organic aerosol at a southeastern US location. Atmos. Environ. 41 (37), 8288–8300.
Li, N., Fu, T.-M., Cao, J., Lee, S., Huang, X.-F., He, L.-Y., Ho, K.-F., Fu, J.S., Lam, Y.-F., 2013. Sources of secondary organic aerosols in the Pearl River Delta region in fall: contributions from the aqueous reactive uptake of dicarbonyls. Atmos. Environ. 76 (0), 200–207.
Matsui, H., Koike, M., Kondo, Y., Takami, A., Fast, J., Kanaya, Y., Takigawa, M., 2014. Volatility basis-set approach simulation of organic aerosol formation in East Asia: implications for anthropogenic–biogenic interaction and controllable amounts. Atmos. Chem. Phys. 14 (18), 9513–9535.
Miyazaki, Y., Kondo, Y., Takegawa, N., Komazaki, Y., Fukuda, M., Kawamura, K., Mochida, M., Okuzawa, K., Weber, R.J., 2006. Time-resolved measurements of water-soluble organic carbon in Tokyo. J. Geophys. Res. Atmos. 111 (D23), D23206.
Odum, J.R., Hoffmann, T., Bowman, F., Collins, D., Flagan, R.C., Seinfeld, J.H., 1996. Gas/particle partitioning and secondary organic aerosol yields. Environ. Sci. Technol. 30 (8), 2580–2585.
Pankow, J.F., 1994. An absorption model of the gas/aerosol partitioning involved in the formation of secondary organic aerosol. Atmos. Environ. 28 (2), 189–193.
Robinson, A.L., Donahue, N.M., Shrivastava, M.K., Weitkamp, E.A., Sage, A.M., Grieshop, A.P., Lane, T.E., Pierce, J.R., Pandis, S.N., 2007. Rethinking organic aerosols: semivolatile emissions and photochemical aging. Science 315, 1259–1262.
Skamarock, W.C., Klemp, J.B., Dudhia, J., Gill, D.O., Barker, D.M., Duda, M., Huang, X.-Y., Wang, W., Powers, J.G., 2008. A Description of the Advanced Research WRF Version 3. NCAR Technical Note.
Wang, J.-L., Chew, C., Chang, C.-Y., Liao, W.-C., Lung, S.-C.C., Chen, W.-N., Lee, P.-J., Lin, P.-H., Chang, C.-C., 2013. Biogenic isoprene in subtropical urban settings and implications for air quality. Atmos. Environ. 79 (0), 369–379.
Zhang, Q., et al., 2007. Ubiquity and dominance of oxygenated species in organic aerosols in anthropogenically-influenced Northern Hemisphere midlatitudes. Geophys. Res. Lett. 34 (13), L13801.
Zhang, Q., Streets, D.G., Carmichael, G.R., He, K., Huo, H., Kannari, A., Klimont, Z., Park, I., Reddy, S., Fu, J., 2009. Asian emissions in 2006 for the NASA INTEX-B mission. Atmos. Chem. Phys. 9 (14), 5131–5153.
Zhao, J., Levitt, N.P., Zhang, R.Y., Chen, J.M., 2006. Heterogeneous reactions of methylglyoxal in acidic media: implications for secondary organic aerosol formation. Environ. Sci. Technol. 40, 7682–7687.